ARTICLE

Electronic Structure and Circular Dichroism of Natural Alboatisins Isolated from Aerial Parts of *Isodon Albopilosus*: DFT and TDDFT Study

Gao-zhang Gou[a,b*], Bo Zhou[a], Ling Shi[a], Shao-ming Chi[c], Xian-lan Chen[a], Wei Liu[a,b*]

a. School of Science, Honghe University, Mengzi 661199, China
b. Key Laboratory of Natural Pharmaceutical and Chemical Biology of Yunnan Province, Mengzi 661199, China
c. College of Chemistry and Chemical Engineering, Yunnan Normal University, Kunming 650500, China

(Dated: Received on March 19, 2015; Accepted on July 14, 2015)

The stable conformations of a series of bioactive molecules, (−)-alboatisins A−C, are identified via Monte Carlo searching with the MMFF94 molecular mechanics force field. Then, the optical rotation (OR) values, vibrational circular dichroism (VCD), and electronic circular dichroism (ECD) spectra were calculated using the gradient-corrected density functional theory method. The vibrational and transition modes of molecular chirality were explored in terms of their microscopic origin. The calculated specific rotations are in agreement with the experimental values. From the OR analysis, it was concluded that optical rotation values are regulated by hydroxyl substitution. Vibrations occurring on the chiral skeleton may cause strong absorption in VCD spectra; VCD spectra are thus the spectral response to deformation vibrations on the chiral carbon skeleton. The lowest-energy negative Cotton effect is caused by $\sigma \rightarrow \pi^*$ transition. Frontier molecular orbital analysis showed that strong ECD absorptions are produced when the dominant transition on the chiral skeleton is asymmetric; ECD spectra show the result of transitions lacking asymmetry on the chiral skeleton.

Key words: Alboatisin, Optical activity, Density functional theory, Circular dichroism, Cotton effect

I. INTRODUCTION

As evidenced by the rich diversity of chiral molecules present in living systems, researches on chirality have become significant subjects since different chiral isomers of numerous pesticides, medicines, cosmetics, and health foodstuffs exhibit different bioactivities through their interactions with other chiral bio-macromolecules such as nucleotides, proteins, and DNA [1]. Chirality is one of the most important properties in nature, and chiral molecules playing an extremely important role [2].

Optical isomers differ in their optical properties such as their optical rotation (OR) values and circular dichroism (CD) spectra. CD is a powerful chiral spectroscopic tool [3] with application toward the configurational/conformational analysis of chiral molecules with mirror-image enantiomers used for chiral recognition processes, asymmetric syntheses, asymmetric catalysis, protein folding, and chiral molecular nanodevices [4–6]. Theoretical studies of chiral compounds are thus highly useful in applications involving chiral molecular recognitions, separations, syntheses, sensing, and catalysis.

In 2007, three biogenetically interesting ent-kauranederived metabolites, (−)-alboatisins A−C (Fig.1) featuring a C13-oxygenated ent-atisane skeleton, were isolated from the aerial parts of *Isodon albopilosus*. Compound B exhibited cytotoxicity against A549 and HT-29 human cancer cells, with IC_{50} values of 8.3 and 7.9 μmol/L, respectively [7]. In the present work, we utilized the DFT method to optimize the molecular geometry of the electronic ground state for (−)-alboatisins ACC, and calculated the IR and VCD spectra for each compound. A TDDFT approach is also employed to calculate the properties of the electronically excited states, as well as their UV-Vis and ECD spectra. We explored the dependence of molecular geometry and electronic structure on the different patterns exhibited by the respective VCD and ECD spectra for each compound. The specific rotation, as one of the most important qualities of a chiral system, is also calculated and compared with experimental values.

II. COMPUTATIONAL DETAILS AND THEORY

The popular quantum chemistry software Gaussian 09W [8] was used to implement the present computational study. According to the electromagnetic field

*Authors to whom correspondence should be addressed. E-mail: liuwei4728@163.com, hhxylxyhxx@126.com

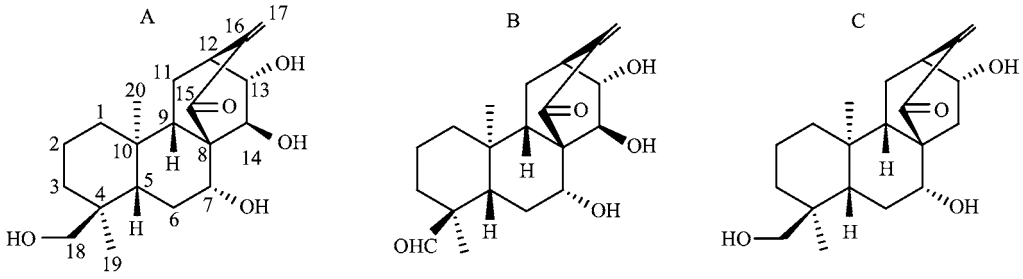

FIG. 1 Schematic structures of (−)-alboatisins A−C.

theory [9], CD is a phenomenon that originates from the differences in absorption of left-circularly-polarized (LCP) and right-circularly-polarized (RCP) radiation when a beam of plane polarized light passes through chiral material. The molar extinction coefficient differential $\Delta\varepsilon(\nu)$ of longitudinal coordinates in the VCD spectrum is expressed as follows:

$$\Delta\varepsilon(\nu) = 4.35 \cdot 1038\nu \sum R_j f_j(\nu_j) \tag{1}$$

$$R_j = \mathrm{Im}\left[\langle g|\mu_{\mathrm{el}}|j\rangle \langle j|\mu_{\mathrm{mag}}|g\rangle\right] \tag{2}$$

here, $f_j(\nu_j)$ is the normalized Lorentz peak function, and ν is the incident light frequency. R_j is the rotation strength of electronic vibrational energy when vibrational energy jumps from g to j under frequency ν_j. μ_{el} and μ_{mag} represent the vibration electric dipole and vibration magnetic dipole, respectively. The numerical value is equal to the imaginary dot product of the vibration electric dipole moment $\langle|g|\mu_{\mathrm{el}}|j\rangle$ and vibration magnetic dipole moment $\langle j|\mu_{\mathrm{mag}}|g\rangle$. Under the nuclear wave function approximations, the value of R_j can be withheld by calculating the linear molecular electric oscillation and magnetic oscillation angle caused by atomic displacements. R_j is used to plot the VCD spectra, with both vibration and fundamental vibration frequencies corrected by the factor 0.962. In the VCD spectrum, positive and negative R_j values show a positive and negative Cotton effect, respectively.

Both electric and magnetic transition dipoles are treated in the quantum mechanical calculations of electronically excited states, followed by the deduction of rotatory strength (R_e) for excitation number e out of the ground state, according to the imaginary part of the point multiplication of the electric and magnetic transition dipoles:

$$R_e = \mathrm{Im}\left[d_j \cdot m_j^*\right] \tag{3}$$

$$d_j = \langle\Psi_0|d|\Psi_j\rangle \tag{4}$$

$$m_j = \langle\Psi_0|m|\Psi_j\rangle \tag{5}$$

where d_j is the electric transition dipole vector and m_j denotes the magnetic transition dipole vector. The specific rotation, $[\alpha]_\omega$, with incident light of frequency ω is then calculated in terms of the optical rotatory parameter $\beta(\omega)$:

$$\beta(\omega) = \frac{2c}{3} \sum \frac{R_e}{{\omega_e}^2 - \omega^2} \tag{6}$$

$$[\alpha]_\omega = 7200 \frac{\omega^3 N_{\mathrm{A}}}{c^2 M} \beta(\omega) \tag{7}$$

where ω is the frequency of the incident polarized light and ω_λ denotes the vertical transition frequency. Further computational details for these equations can be found in the literature [10–15].

Conformational analysis of alboatisins A−C was carried out as follows. Initially, stable conformations were identified via Monte Carlo searching with the MMFF94 molecular mechanics force field using the SPARTAN 02 program [16]. In each case the minimum energy structures were filtered and checked for duplicity. The energy cutoff of 6 kcal/mol was selected in order to have a wide window of conformers in the Boltzmann distribution. Nine conformers were searched for compound A and 3, 9 conformers were searched for compounds B, C, respectively. The conformation structures are shown in Fig.2. All conformations are then reoptimized using the DFT method combined with the B3LYP exchange-correlation functional [17–19] at the 6-311++G** by the Gaussian 09 program [8]. The total molecular energies and OR values were calculated at the same level, see Table S1 in supplementary materials. Then, the conformation that the OR values were close to the experimental value was selected. Next, their OR, infrared spectra (IR) and VCD spectra were calculated at the B3LYP/6-31+G* level. In cases where computational conditions allow, we also used an extended double-zeta splitting basis set, 6-311++G** [20–22]. The electronically excited states involving the first 30 excited states of alboatisins A−C were calculated using the TDDFT method. In all calculations, squeezed self-consistent field (SCF) convergence standards were adopted. In order to be compared with the experimental data, the self-consistent reaction field (SCRF) method and polarized continuum model (PCM) [23, 24] were used to optimize their geometries and calculate their UV-Vis spectra in methanol at the 6-311++G** level.

According to the calculated absorption frequency val-

DOI:10.1063/1674-0068/28/cjcp1503045

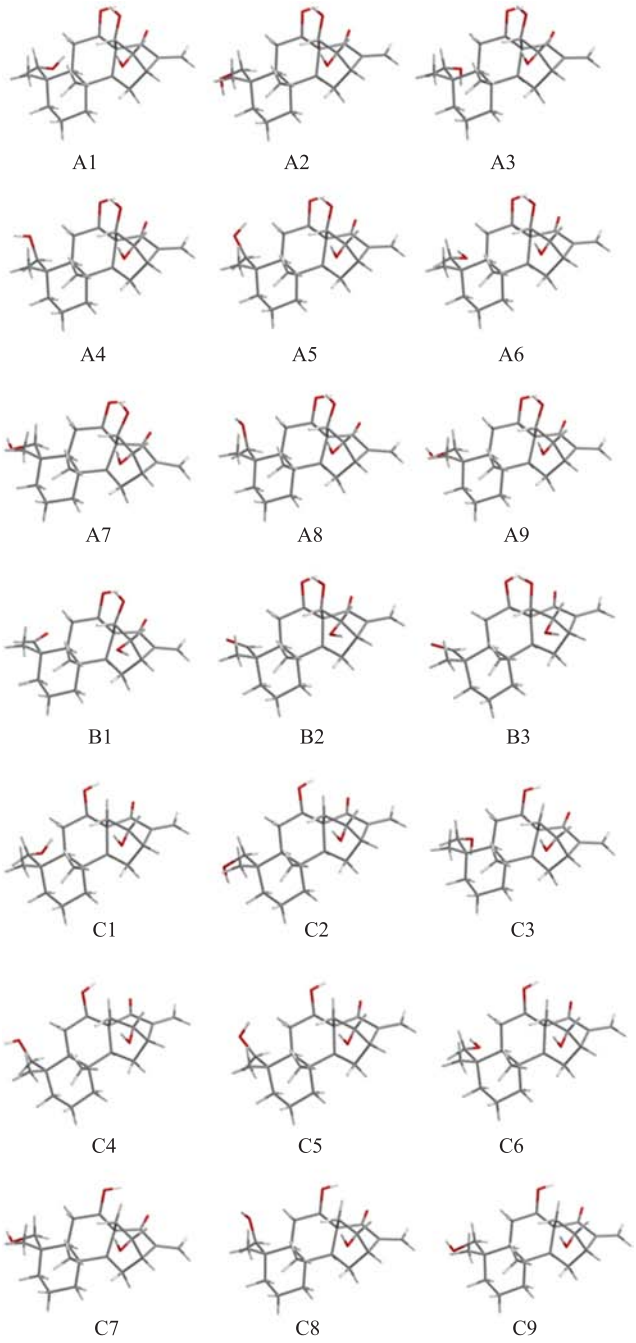

FIG. 2 The stable conformation structures of (−)-alboatisins A−C searched by Spartan 02 program.

ues, infrared vibrational strength, and rotatory strength calculated under 6-311++G** level, the IR and VCD spectra were simulated with peaks of 15 cm^{-1} at half-width having Lorentzian characteristics. On the basis of rotational strengths, transition dipole strengths, and absorption maxima, the UV-Vis and ECD spectra were fitted with a Lorentzian linear shape of 10 nm half-width.

TABLE I Calculated and experimental specific rotations of alboatisins A−C using 589.0 or 0.0 nm line.

Item		6-31+G*	6-311++G**	6-311++G**[a]	Expt.[b]
A3 $[\alpha]_D^0$	(−)	−63.34	−81.21	−37.38	
	(+)	+63.34	+81.21	+37.38	
$[\alpha]_D^{20}$	(−)	−65.14	−58.81	−20.93	−18.6
	(+)	+65.14	+58.81	+20.93	
B1 $[\alpha]_D^0$	(−)	−53.54	−12.01	−19.51	
	(+)	+53.54	+12.01	+19.51	
$[\alpha]_D^{20}$	(−)	−23.33	−17.51	−0.57	−16.7
	(+)	+23.33	+17.51	+0.57	
C3 $[\alpha]_D^0$	(−)	−78.26	−70.51	−71.24	
	(+)	+78.26	+70.51	+71.24	
$[\alpha]_D^{20}$	(−)	−56.95	−44.72	−33.18	−34.7
	(+)	+56.95	+44.72	+33.18	

[a] Calculated by the PCM model in MeOH at 6-311++G** level.
[b] Determinated in MeOH [7].

III. RESULTS AND DISCUSSION

A. Optical rotation

As shown in Fig.1, Fig.2, and Fig.S1 (supplementary materials), the structures of (−)-alboatisins A−C share similarities in their diterpenoid skeletons, except for substitution at C18 and C14, with most -OH functional groups located on the chiral carbon skeleton [7]. The experimentally obtained $[\alpha]_D^{20}$ values of naturally occurring (−)-alboatisins A−C are −18.6°, −16.7°, and −34.7°, respectively [7]. As shown in Table S1 (supplementary materials), the total molecular energies of every stable conformers for (−)-alboatisins A−C were very close. Among them, the calculated specific rotations of conformers A3, B1, and C3 are the most close to the experimental values. All the computational specific rotations, $[\alpha]_D^{20}$, for conformers A3, B1, and C3 are summarized in Table I, together with their reported values. Calculated values of $[\alpha]_D^{20}$ for conformers A3, B1, and C3 were −20.93°, −17.51°, −33.18° and close to the experimental values. From a qualitative standpoint, the calculated OR magnitudes of (−)-alboatisins A−C were consistent with experimental values. A solvent effect was attributed to the substantial reduction in OR values. Comparing alboatisin A with C from a molecular structure standpoint, the OR decrease about 13° because C lacked an -OH group present at C14 in A. This lack of a chiral -OH group appears to diminish the OR significantly; OR values are regulated by OH substitution. Comparing alboatisin A with B, the introduction of a -CHO group on C18 can accommodate additional electronic charge and strengthen the chiral characteristics, as evidenced by an increased OR value for A.

DOI:10.1063/1674-0068/28/cjcp1503045

TABLE II Calculated and experimental IR and VCD spectral data of (−)-alboatisins A3 at the B3LYP/6-311++G** level (ν in cm^{-1} and I in km/mol).

Mode	ν	I	R_j	Expt.[a]	Assignment
ν_1	3689	46.7	6.23	3424	ν(OH)
ν_2	3624	71.3	−1.90	3424	ν(OH)
ν_3	3532	177.1	52.9	3424	ν(OH)
ν_4	2953	53.0	−20.9		ν_s(CH_3)
	2939	56.1	8.1	2925	ν_{as}(CH_2)
	2934	33.1	62.8		ν_{as}(CH_2)
	2856	51.4	4.7	2872	ν_s(CH_2OH)
ν_5	1686	117.7	4.81	1711	ν(C=O)
ν_6	1618	72.2	−8.4	1632	ν(C=C)
ν_1	1474	13.0	−24.9	1464	δ(CH_3)
ν_8	1463	5.7	20.4	1444	δ(CH_2)
	1389	12.3	80.9	1390	ν(C−C)
	1366	6.2	−29.5		δ(CH_2, CH_3)
	1356	11.7	−21.0	1342	δ(CH_2, CH_3)
	1355	28.4	−58.4	1304	δ(CH_2, OH)
ν_9	1258	13.0	75.4		δ(C−H)
	1254	6.2	48.6		δ(OH)
ν_{10}	1149	31.5	−66.6	1152	δ(C−H, OH)
	1140	16.3	−50.8		δ(C−H, OH)
ν_{11}	1135	29.4	50.4		ν_{as}(C−C)
ν_{12}	1071	70.1	−134	1052	ν_{as}(C−C)
ν_{13}	1058	75.5	117	1037	ν_{as}(C−C)
ν_{14}	694	78.8	67.3		δ(OH)
ν_{15}	564	6.2	−34.1		γ(C−H)

[a] Experimental data of ν were measured in CH_3OH [7].

TABLE III Calculated and experimental IR and VCD spectral data of (−)-alboatisins B1 at the B3LYP/6-311++G** level (ν in cm^{-1} and I in km/mol).

Mode	ν	I	R_j	Expt.[a]	Assignment
ν_1	3695	45.3	−6.6		ν(OH)
ν_2	3629	70.6	−3.8		ν(OH)
ν_3	3538	173.1	53.1	3452	ν(OH)
ν_4	2959	21.9	60.5	2933	ν_s(CH_3)
	2946	23.1	83.1	2854	ν_{as}(CH_2)
ν_5	2737	78.8	29.7		ν (CHO)
ν_6	1730	248.2	−23.5	1727	ν(C=O)
ν_7	1688	119.2	−4.8	1706	ν(C=O, C=C)
ν_8	1618	68.1	−6.5	1632	ν(C=C)
ν_9	1471	10.0	−28.4	1444	δ(CH_3)
ν_{10}	1380	15.6	−60.1	1397	ν(CDC)
	1374	14.1	−10.3	1385	δ(CH_2, CH_3)
ν_{11}	1272	10.1	−26.9		δ(CH_2, CH_3)
	1254	27.6	−95.8		δ(CH_2)
	1229	20.8	−40.0		δ(CH_2, CH_3)
ν_{12}	1059	36.3	70.1	1099	ν_{as}(C−C)
	1057	36.6	16.1	1063	ν_{as}(C−C)
	1008	63.7	47.4	1036	ν_{as}(C−C)
	1005	25.9	−46.3		ν_{as}(C−C)
ν_{13}	952	34.2	−58.2		γ(C−H)
ν_{14}	840	9.3	69.9		γ(C−H)
ν_{15}	689	79.2	48.3		δ(OH)

[a] Experimental data of ν were measured in CH_3OH [7].

Whether attributed to the lower level of precision for (B3LYP/6-31+G*) or the higher level of accuracy for (B3LYP/6-311++G**), the calculated OR values were not equal to experimental values. This difference between theoretical and experimental results may be caused by three factors. The first may be the drawback of the computational methodology employed, such as the imprecise and incomplete functional and basis set used. Therefore, if we use a complete basis set for calculations, the calculated value is likely to decrease and shows greater convergence with experimental values. A second reason may be that the calculated OR could be the most stable conformer, but the experimental specimen consists of a mixture containing some sub-stable or unstable conformer. A discussion of optical rotation by sum contributions of all possible conformers in principle is required. The third factor for consideration is that the enantiomeric excess (ee) values for experimental samples were not to be reminded when determining OR values, and the mutual transformation of optical isomers was not considered. The OR determined would be smaller if the sample contains a certain amount of racemic modification.

B. VCD spectra

The IR and VCD spectra calculated under B3LYP/6-311++G** level of the stable conformers A3, B1, C3 are shown in Fig.3 and Tables II−IV. And the simulated spectra calculated under B3LYP/6-31+G* or PCM/B3LYP/6-311++G** level are shown in Fig.S2 and Fig.S4 (supplementary materials). All compounds exhibited about 15 absorption peaks. The symbol ν was used to assign the spectral peaks of (−)-alboatisin conformer A3 (Fig.3(a)). Above 3500 cm^{-1}, peaks ν_1 to ν_3 originated from ν(OH). The infrared intensity was large; however, rotating strength was small because the OH group was away from the chiral skeleton, and a medium intensity absorption peak in VCD spectra showed a moderate positive Cotton effect. The peak corresponding to ν_4 was contributed to a group of close vibration absorptions originating from ν_s(C−H) or ν_{as}(C−H) at a distance from the chiral skeleton, which rendered a less negative and positive Cotton effect, respectively. Peaks attributed to ν_5 and ν_6 originated from ν(C=O) and ν(C=C) extension vibrations, and were characterized by strong IR and weak VCD vibrations not on the chiral skeleton. Peaks ν_7−ν_{11} were

DOI:10.1063/1674-0068/28/cjcp1503045

TABLE IV Calculated and experimental IR and VCD spectral data of (−)-alboatisins C3 at the B3LYP/6-311++G** level (ν in cm^{-1} and I in km/mol).

Mode	ν	I	R_j	Expt.[a]	Assignment
ν_1	3691	38.2	5.9	3448	ν(OH)
ν_2	3649	56.3	−27.0		ν(OH)
ν_3	2937	46.3	−66.7	2930	ν_{as}(C−H)
ν_4	2932	34.8	68.6	2858	ν_s(C−H)
ν_5	1685	119.5	13.0	1710	ν(C=O, C=C)
ν_6	1617	73.3	−8.6	1632	ν(C=C)
ν_7	1472	8.0	−3.2		$\delta(CH_3)$
	1448	11.8	−12.7	1444	$\delta(CH_3)$
ν_8	1380	9.5	−30.1	1398	$\delta(CH_3)$
	1369	8.4	−57.0	1387	ν(C−C)
ν_9	1258	6.9	43.1		$\delta(CH_2)$
	1252	8.5	46.5		$\delta(CH_2)$
ν_{10}	1161	21.9	49.0		δ(C−H)
	1149	20.8	−56.1		ν(C−C)
	1140	18.6	−52.1		ν(C−C)
ν_{11}	1074	17.7	−96.6	1066	ν(C−C)
	1061	21.8	50.2	1046	ν(C−C)
	1034	12.0	26.4		ν(C−C)
ν_{12}	1008	48.1	−124		ν(C−C)
ν_{13}	979	99.0	56.0		ν(C−C)
ν_{14}	957	13.6	22.7		γ(C−H)
ν_{15}	597	22.2	53.4		δ(OH)

[a] Experimental data of ν were measured in CH_3OH [7].

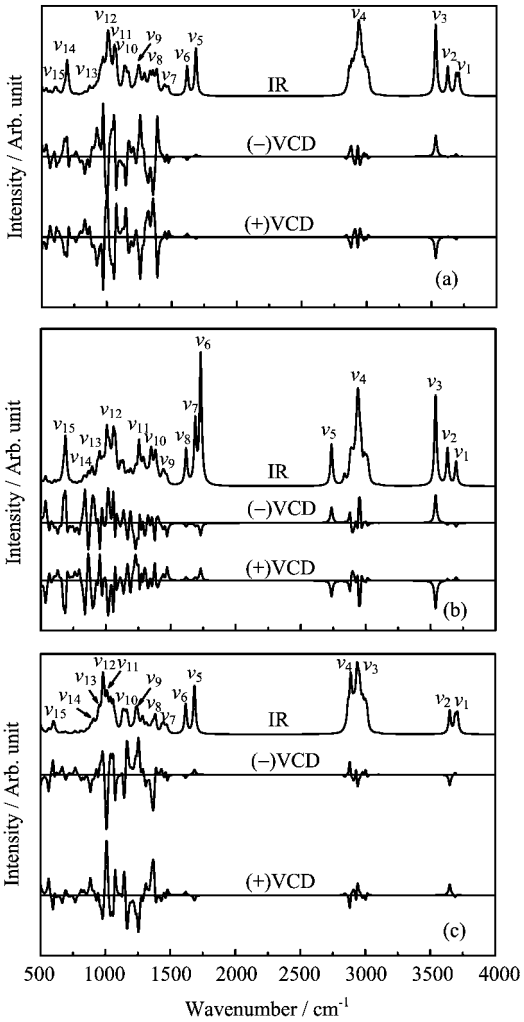

FIG. 3 Simulated IR and VCD spectra of (−)-alboatisin conformer (a) A3, (b) B1, and (c) C3 at the B3LYP/6-311++G** level.

assigned to chiral skeleton extensions such as ν(C−C), $\delta(CH_2)$, *etc.* characterized by weak IR and strong VCD, and showed different intensities corresponding to either a positive or negative Cotton effect. Peaks attributed to ν_{12} and ν_{13} possessed a strong negative and strong positive Cotton effect, respectively, most likely originating from the ν_{as}(C−C) of the chiral skeleton. Peaks ν_{14} to ν_{15} were assigned respectively to γ(C−H) or δ(OH), and their IR and VCD peaks were all weak.

Figure 3(b) depicts the evolution of IR and VCD spectra of (−)-alboatisin conformer B1 at the B3LYP/6-311++G** level. The origin of VCD was similar to that calculated for (−)-alboatisin conformer A3. Peaks ν_1−ν_3 assigned to ν(OH) were accompanied by a weak VCD as a result of its location away from a chiral center. Peak ν_3 showed a medium-intensity positive Cotton effect. The peak attributed to ν_4 originated from ν_{as}(C−H) away from the chiral skeleton and rendered a weak negative or positive Cotton effect. Peaks ν_5−ν_8 exhibited strong IR signals and weak VCD originating from ν(C=O) and ν(C=C) outside of the chiral skeleton. Peaks attributed to ν_9−ν_{12} were chiral skeleton extensions such as ν(C−C), $\delta(CH_2)$, and δ(C−H), and showed a positive or negative Cotton effect of different intensities in the VCD spectrum. Peaks ν_{13} and ν_{14} showed strong negative and strong positive Cotton effect, respectively, largely originating from ν_{as}(C−C) on the chiral skeleton, followed by a γ(C−H) vibration. Peak ν_{15} originated from a δ(OH) vibration.

As shown in Fig.3(c) and Table IV, peaks ν_1 and ν_2 of (−)-alboatisin conformer C3 emerged in the vicinity of 3600 cm^{-1}, originating from ν(OH); the experimental value is 3348 cm^{-1} [7]. From 2800−3000 cm^{-1}, ν_3 and ν_4 originated from ν_{as}(C−H) and rendered weak negative or positive Cotton effects. Peaks ν_5 and ν_6 originated from ν(C=O) and ν(C=C) and showed strong IR absorption with weak VCD. Peaks ν_7−ν_{13} involved several weak IR peaks originating from a chiral skeleton extension, *e.g.*, ν(C−C), $\delta(CH_2)$, and δ(C−H), and showed a positive or negative Cotton effect of different intensities in the VCD spectrum. Peaks ν_{14} and ν_{15} originated from γ(C−H) or δ(OH) vibration and

DOI:10.1063/1674-0068/28/cjcp1503045

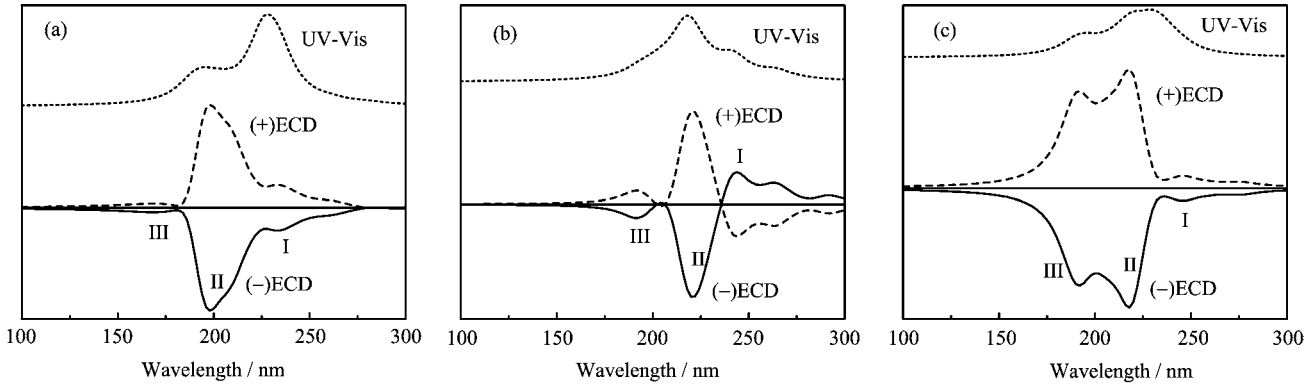

FIG. 4 Simulated UV-Vis and ECD spectra of (−)-alboatisin conformer (a) A3, (b) B1, and (c) C3 at the B3LYP/6-311++G** level. I, II, and III show three absorption bands.

showed weak IR absorptions and VCD.

The above discussions show that the stable conformers for (−)-alboatisins A−C have identifiable spectral areas in which ν(OH) occurs (greater than 3500 cm^{-1}) and show a Cotton effect of medium intensity in the VCD spectra. ν_{as}(C−H) emerged from 2800−3000 cm^{-1} showed either a weak negative or positive Cotton effect. ν(C=C) and ν(C=O) were found to arise from 1600−1750 cm^{-1}, and displayed a weak VCD absorbance. Therefore, we may conclude as follows: the vibrations occurring on the chiral skeleton may appear as strong absorptions in the VCD spectrum and emerge as weak or nonexistent absorption in the IR spectrum, or vice versa. In short, the VCD spectrum can be considered the spectral response to deformation vibrations on the chiral skeleton.

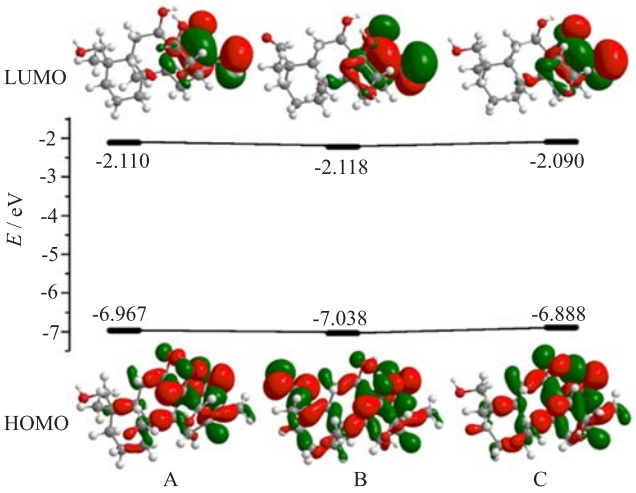

FIG. 5 Molecular orbital energy diagrams and isodensity surface plots of the HOMO and LUMO of (−)-alboatisins A−C at the B3LYP/6-311++G** level.

C. ECD spectra

Calculated UV-Vis and ECD spectra of (−)-alboatisin conformers are shown in Table V and Fig.4. Figure 4(a) depicts the evolution of the UV-Vis and ECD spectra of conformer A3 at the B3LYP/6-311++G** level. And the simulated UV-Vis and ECD spectracal culated under B3LYP/6-31+G* or PCM/B3LYP/6-311++G** level are shown in Fig.S3 and S5 of supplementary materials. The ECD spectrum exhibits three absorption bands (I, II, III); bands I and II are weak in intensity, while band III is strong. Band I renders a medium-strength negative absorption peak in the ECD spectrum, and corresponds to the strongest UV-Vis absorption (calculated maximum UV-Vis absorption of 236 nm), which originated from the $S_0 \rightarrow S_7$ transition induced by HOMO-5 to LUMO($\pi \rightarrow \pi^*$). The molecular orbital energy diagrams and isodensity surface plots of the highest occupied molecular orbitals (HOMOs) and lowest unoccupied molecular orbitals (LUMOs) of stable conformers for (−)-alboatisins A−C are shown in Fig.5. The HOMO charge density crosses the entire molecular skeleton, while the LUMO is focused on C=O or C=C(π^*); thus it shows a medium-strength negative Cotton effect. (−)-Alboatisin A shows a strong negative Cotton effect appearing as band II, which stemmed from the $S_0 \rightarrow S_{15}$ (HOMO-3 to LUMO+1 ($\sigma \rightarrow \pi^*$)) electronic transition that takes place over the whole molecular skeleton and lacks asymmetry. Band III shows the lowest-energy negative Cotton effect caused by the $S_0 \rightarrow S_{23}$ transition, which arose from HOMO to LUMO+6 ($\sigma \rightarrow \sigma^*$).

For (−)-alboatisin conformer B1 (Fig.4(b) and Table V), band I is attributed to the $S_0 \rightarrow S_6$ transition, which contributes to the medium-strength positive Cotton effect stemming from HOMO-4 to LUMO ($\pi \rightarrow \pi^*$). The $S_0 \rightarrow S_9$ of (−)-alboatisin B contributes to the highest-energy negative Cotton effect corresponding to the maximum absorption wavelength (219 nm) in the UV-Vis spectrum, which stemmed from HOMO-

DOI:10.1063/1674-0068/28/cjcp1503045

TABLE V Calculated and experimental UV-Vis and ECD spectral data of (−)-alboatisins A−C at the B3LYP/6-311++G** level.

Band	Conformer	Method	λ/nm	f	R_e	Expt.[a]	Assignment
I	A3	B3LYP/6-31+G*	227	0.15	−6.1		$S_0 \rightarrow S_7$, HOMO-5→LUMO ($\pi \rightarrow \pi^*$)
		B3LYP/6-311++G**	231	0.14	−3.9	236	
		PCM/B3LYP/6-311++G**	232	0.18	−0.13		
	B1	B3LYP/6-31+G*	244	0.06	6.4		$S_0 \rightarrow S_6$, HOMO-4→LUMO ($\pi \rightarrow \pi^*$)
		B3LYP/6-311++G**	241	0.06	7.3		
		PCM/B3LYP/6-311++G**	245	0.05	13.6		
	C3	B3LYP/6-31+G*	247	0.01	−4.9		$S_0 \rightarrow S_4$, HOMO-5→LUMO ($\pi \rightarrow \pi^*$)
		B3LYP/6-311++G**	245	0.01	−4.1		
		PCM/B3LYP/6-311++G**	242	0.02	−3.7		
II	A3	B3LYP/6-31+G*	195	0.01	−24.6		$S_0 \rightarrow S_{15}$, HOMO-3→LUMO+1 ($\sigma \rightarrow \pi^*$)
		B3LYP/6-311++G**	198	0.003	−15.1		
		PCM/B3LYP/6-311++G**	195	0.02	−16.6		
	B1	B3LYP/6-31+G*	221	0.14	−33.2		$S_0 \rightarrow S_9$, HOMO-6→LUMO ($\sigma \rightarrow \pi^*$)
		B3LYP/6-311++G**	219	0.14	−32.5	234	
		PCM/B3LYP/6-311++G**	228	0.19	−31.3		
	C3	B3LYP/6-31+G*	220	0.09	−34.1		$S_0 \rightarrow S_8$, HOMO-7→LUMO ($\sigma \rightarrow \pi^*$)
		B3LYP/6-311++G**	219	0.09	−36.7	234	
		PCM/B3LYP/6-311++G**	226	0.09	−37.0		
III	A3	B3LYP/6-31+G*	185	0.01	−9.9		$S_0 \rightarrow S_{23}$, HOMO→LUMO+6 ($\sigma \rightarrow \sigma^*$)
		B3LYP/6-311++G**	188	0.006	−1.2		
		PCM/B3LYP/6-311++G**	186	0.02	−3.4		
	B1	B3LYP/6-31+G*	189	0.005	−5.0		$S_0 \rightarrow S_{24}$, HOMO→LUMO+5 ($\sigma \rightarrow \sigma^*$)
		B3LYP/6-311++G**	192	0.005	−5.3		
		PCM/B3LYP/6-311++G**	191	0.002	−5.1		
	C3	B3LYP/6-31+G*	189	0.02	−17.1		$S_0 \rightarrow S_{23}$, HOMO-7→LUMO ($\sigma \rightarrow \pi^*$)
		B3LYP/6-311++G**	190	0.01	−8.7		
		PCM/B3LYP/6-311++G**	197	0.02	−23.1		

[a] Experimental data of λ were measured in CH_3OH [7].

6 to LUMO ($\sigma \rightarrow \pi^*$) that the electronic transition most takes place not in a certain situation. Band III, originating from the $S_0 \rightarrow S_{24}$ transition, stemmed from HOMO to LUMO+5 ($\sigma \rightarrow \sigma^*$) and contributed to the lowest-energy negative Cotton effect.

Similar to (−)-alboatisin conformer B1, bands II and III for (−)-alboatisin conformer C3 (Fig.4(c)) show a negative Cotton effect, and band II is the strongest in the ECD spectrum. Band I, contributed by the $S_0 \rightarrow S_4$ transition at 245 nm, arose from HOMO-5 to LUMO ($\pi \rightarrow \pi^*$). Band II, which corresponds to the maximum absorption wavelength (219 nm) in the UV-Vis spectrum, originated from the $S_0 \rightarrow S_8$ transition induced by HOMO-7 to LUMO ($\sigma \rightarrow \pi^*$). Figure 5 shows a three-dimensional representation of the main LUMOs contributing to the highest-energy negative Cotton effect; band III stemmed from the $S_0 \rightarrow S_{23}$ transition and shows a medium-strength negative Cotton effect originating from HOMO-7 to LUMO ($\sigma \rightarrow \sigma^*$).

In Table V, the calculated maximum absorption wavelength is consistent with the experimental value. However, if the dominant transition lacks asymmetry on the chiral skeleton, the UV-Vis spectrum may be small and the ECD spectrum may be large. Conversely, if the dominant transition exhibits asymmetry on the chiral skeleton, the UV-Vis spectrum may be strong and the ECD spectrum may be weak. The ECD spectrum can thus be considered to represent the spectral response to transitions lacking asymmetry on the chiral skeleton.

IV. CONCLUSION

In the present work, three biogenetically interesting ent-kaurane-derived metabolites, (−)-alboatisins A−C have been studied by conformational analysis, optimization of their conformer structures. OR values IR, VCD, ECD, UV-Vis spectra and molecular orbital energies were calculated using a DFT method. Their IR and UV-Vis spectra and OR values were in good accordance

DOI:10.1063/1674-0068/28/cjcp1503045

with reported experimental values. Molecular structure analysis suggests that the OR values are regulated by hydroxyl (-OH) substitution on the chiral carbon skeleton. Furthermore, vibrations occurring on the chiral skeleton may cause strong absorptions in the VCD spectra, which manifest as weak or nonexistent absorption in the corresponding IR spectra. Thus, the VCD spectrum can be interpreted as the spectral response occurring from deformation vibrations on the chiral skeleton. The lowest-energy negative Cotton effect exhibited by (−)-alboatisins A−C is caused by a $\sigma \rightarrow \pi^*$ transition. Frontier molecular orbital analysis reveals that a strong ECD absorption is produced when the dominant transition on the chiral skeleton is asymmetric. Accordingly, the ECD spectrum can be described as the spectral response to transitions lacking asymmetry on the chiral skeleton.

Supplementary materials: The IR, UV-Vis, VCD and ECD spectra calculated at B3LYP/6-31+G* and PCM-B3LYP/6-311++G** levels of theory for stable conformers of Alboatisins A3, B1, C3 in gas and methanol medium (Figs.S2−S5), the experimental and calculated specific rotations of every stable conformers for alboatisins A−C using the sodium D line under 6-311++G** level (Table S1).

V. ACKNOWLEDGMENTS

This work is supported by the National Natural Science Foundation of China (No.61361002 and No.21262049), the "Chun Hui" Plan of Chinese Ministry Education (No.Z2011125), the Scientific Research Foundation of Education Department of Yunnan Province (No.2013FZ121), the Youth Program of Yunnan Province (No.2014FD054), the Chemistry of Key Construction Disciplines for Master Degree Program in Yunnan (No.HXZ1303), and the Educational Reform Program of Honghe University (No.JJJG1412), the General Program of Yunnan Provincial Education Departmen (No.2015Y455).

[1] C. Y. Mang, Z. G. Li, and K. C. Wu, Chin. Phys. B **19**, 043601 (2010).
[2] C. Brückner, D. C. Götz, S. P. Fox, C. Ryppa, J. R. McCarthy, T. Bruhn, J. Akhigbe, S. Banerjee, P. Daddario, and H. W. Daniell, J. Am. Chem. Soc. **133**, 8740 (2011).
[3] M.Górecki, A. Karczmarska-Wódzka, R. Kołodziejska, M.Dramiński, and J. Frelek, Eur. J. Org. Chem. **2014**, 5204 (2014).
[4] F. Formaggio, C. Peggion, M. Crisma, B. Kaptein, Q. B. Broxterman, J. P. Mazaleyrat, M. Wakselman, and C. Toniolo, Chirality **16**, 388 (2004).
[5] L. Dutot, K. Wright, A. Gaucher, M. Wakselman, J. P. Mazaleyrat, M. D. Zotti, C. Peggion, F. Formaggio, and C. Toniolo, J. Am. Chem. Soc. **130**, 5986 (2008).
[6] M. Tanasova, C. Vasileiou, O. O. Olumolade, and B. Borhan, Chirality **21**, 374 (2009).
[7] S. X. Huang, Y. Zhou, L. B. Yang, Y. Zhao, S. H. Li, L. G. Lou, Q. B. Han, L. S. Ding, and H. D. Sun, J. Nat. Prod. **70**, 1053 (2007).
[8] M. J. Frisch, G. W. Trucks, H. B. Schlegel, G. E. Scuseria, M. A. Robb, J. R. Cheeseman, G. Scalmani, V. Barone, B. Mennucci, G. A. Petersson, H. Nakatsuji, M. Caricato, X. Li, H. P. Hratchian, A. F. Izmaylov, J. Bloino, G. Zheng, J. L. Sonnenberg, M. Hada, M. Ehara, K. Toyota, R. Fukuda, J. Hasegawa, M. Ishida, T. Nakajima, Y. Honda, O. Kitao, H. Nakai, T. Vreven, J. A. Jr. Montgomery, J. E. Peralta, F. Ogliaro, M. Bearpark, J. J. Heyd, E. Brothers, K. N. Kudin, V. N. Staroverov, R. Kobayashi, J. Normand, K. Raghavachari, A. Rendell, J. C. Burant, S. S. Iyengar, J. Tomasi, M. Cossi, N. Rega, J. M. Millam, M. Klene, J. E. Knox, J. B. Cross, V. Bakken, C. Adamo, J. Jaramillo, R. Gomperts, R. E. Stratmann, O. Yazyev, A. J. Austin, R. Cammi, C. Pomelli, J. W. Ochterski, R. L. Martin, K. Morokuma, V. G. Zakrzewski, G. A. Voth, P. Salvador, J. J. Dannenberg, S. Dapprich, A. D. Daniels, Ö. Farkas, J. B. Foresman, J. V. Ortiz, J. Cioslowski, and D. J. Fox, *Gaussian 09, Revision B.01*, Wallingford CT: Gaussian, Inc., (2010).
[9] P. Stephens and M. Lowe, Annu. Rev. Phys. Chem. **36**, 213 (1985).
[10] J. P. Simonato, J. Pécaut, and J. C. Marchon, J. Am. Chem. Soc. **120**, 7363 (1998).
[11] C. Y. Mang, C. P. Liu, and K. C. Wu, Mol. Phys. **110**, 1453 (2012).
[12] C. Y. Mang, G. Z. Gou, C. P. Liu, and K. C. Wu, Acta. Phys. Sin. **4**, 131 (2011).
[13] C. Y. Mang, C. P. Liu, and K. C. Wu, Spectrochim. Acta A **98**, 444 (2012).
[14] C. Y. Mang, Y. Zhao, H. F. Li, H. Lan, Y. Yan, and M. H. Yang, Mol. Phys. **113**, 104 (2015).
[15] C. Y. Mang, C. P. Liu, G. M. Liu, B. Jiang, H. Lan, K. C. Wu, and Y. Zhao, Spectrochim. Acta A **136**, 1401 (2015).
[16] B. J. Deppmeier, A. J.Driessen, T. S. Hehre, W. J. Hehre, J. A. Johnson, P. E. Klunzinger, and J. A. Pople, *SPARTAN 02*, Irvine, CA: Wavefunction. Inc., (2002).
[17] A. D. Becke, Phys. Rev. A. **38**, 3098 (1988).
[18] A. D. Becke, J. Chem. Phys. **98**, 5648 (1993).
[19] C. Lee, W. Yang, and R. G. Parr, Phys. Rev. B **37**, 785 (1988).
[20] W. J. Hehre, R. Ditchfield, and J. A. Pople, J. Chem. Phys. **56**, 2257 (1972).
[21] M. M. Francl, W. J. Pietro, W. J. Hehre, J. S. Binkley, M. S. Gordon, D. J. DeFrees, and J. A. Pople, J. Chem. Phys. **77**, 3654 (1982).
[22] R. Krishnan, J. S. Binkley, R. Seeger, and J. A. Pople, J. Chem. Phys. **72**, 650 (1980).
[23] S. Miertuš, E. Scrocco, and J. Tomasi, Chem. Phys. **55**, 117 (1981).
[24] B. Mennucci, E. Cances, and J. Tomasi, J. Phys. Chem. B **101**, 10506 (1997).

DOI:10.1063/1674-0068/28/cjcp1503045